ADVANCED FUNCTIONAL MATERIALS
www.afm-journal.de



# Understanding the Microscopic Origin of the Very High Charge Mobility in PBTTT: Tolerance of Thermal Disorder

*Tao Liu and Alessandro Troisi**

**The one-electron states responsible for hole transport in the high-mobility semicrystalline polymer PBTTT are investigated using a combination of large-scale electronic structure calculations (with the DFTB method) and classical molecular dynamics simulations. The validity of the structural model is established by comparison with the available data from crystallography, including the paracrystallinity parameter. The localization characteristics of the states at the edge of the valence band, their geometry, and their time evolution clearly indicate the characteristics of PBTTT that are at the origin of its improved mobility: i) the orbitals become very rapidly delocalized within few tens of eV from the valence band edge, that is, the density of trap states is low and the mobility edge is very close to the valence band edge; ii) a very large delocalization of states across chains is observed; iii) the traps, determined by local distortions of the chain, have a typical lifetime of less than 0.1 ns, that is, the conformational changes of the polymer due to its thermal fluctuations are sufficient to induce a detrapping of the charge carrier and the traps are "self-healing".**

## 1. Introduction

After many decades of investigation in polymer semiconductors,[1–3] the relation between the microscopic structure of the polymer and its charge mobility remains unclear. One firm point is that charge carriers injected in a semiconducting polymer occupy localized states near the valence (or conduction) edge for hole (or electron). The transport is thermally activated and can be described phenomenologically by different models all based on assumptions on the shape of the density of states, the localization of these states, and the properties of the carriers at different energies.[2,4,5] For amorphous polymers, one of the variants of the variable range hopping methods[4] is used while, for semicrystalline polymers, multiple trapping and release methods have been often adopted with success.[6] In all these models the mobility is largely determined by the energy distribution of the localized states at the band edge with narrow energy distributions being associated with higher mobility.[7] The introduction of P3HT, a polymer characterized by highly ordered crystalline domains and a relatively high mobility ($\mu \approx 0.1$ cm$^2$ V$^{-1}$ s$^{-1}$),[8] seemed to substantiate the hypothesis that increased local order was the key for high mobility. The synthesis and characterization of PBTTT (poly[2,5-bis(3-alkylthiophen-2-yl)thieno(3,2-b)thiophene], shown in **Figure 1**)[9,10] further supported this idea: PBTTT can form highly ordered crystalline domains in three dimensions by lamellar structures of $\pi$-stacking conjugated backbones separated by interdigitated alkyl side chains.[11–13] The formation of such high-quality crystallites has been suggested to be directly related to the better performance of PBTTT in thin film transistors, where the hole mobility reaches $\approx$1 cm$^2$ V$^{-1}$ s$^{-1}$. Another reason for the high promise of PBTTT is the high ionization potential of about 5.1 eV (in comparison that of P3HT is 4.8 eV), which makes PBTTT material more stable against oxidation by oxygen in air.[9]

The highly intuitive and appealing idea that high charge mobilities are associated with high order was shook by the introduction of a number of polymer families[14–16] with no order detectable crystallographically and hole mobility similar or higher to that of PBTTT. In order to understand the factors affecting the mobility at a microscopic level, it is essential to characterize the states responsible for transport (those close to the band edge) for different polymers and, hopefully, draw some general conclusion that can be useful for the synthesis of the new families of polymers. In the case of semicrystalline polymers one should try to understand what the chemical nature is of the localized states at the band edge, an information not present in averaged structures derived from crystallography. When the latter are used to compute the electronic structure, they display fully delocalized orbitals (or very delocalized polaronic states if polaronic effects are included).[17] Understanding the origin of disorder in such ordered phases is a problem that we have first considered for the P3HT polymer[18,19] and that we extend in this paper to the more difficult case of PBTTT by combining MD (molecular dynamic) simulations and large scale electronic structure calculations.

The work presented here should complement the insight obtained by other computational works presented in literature. Focusing on perfectly crystalline structures, first-principles pseudopotential density functional calculations on the atomic and electronic structure of PBTTT have been carried out by Norhtrup.[20] He concluded that substantial interdigitation of the alkyl side chains is energetically favorable for PBTTT, and the higher mobility observed experimentally for PBTTT in

Dr. T. Liu, Prof. A. Troisi
Department of Chemistry and
Centre of Scientific Computing
University of Warwick, CV4 7AL Coventry, UK
E-mail: A.Troisi@warwick.ac.uk

DOI: 10.1002/adfm.201302069

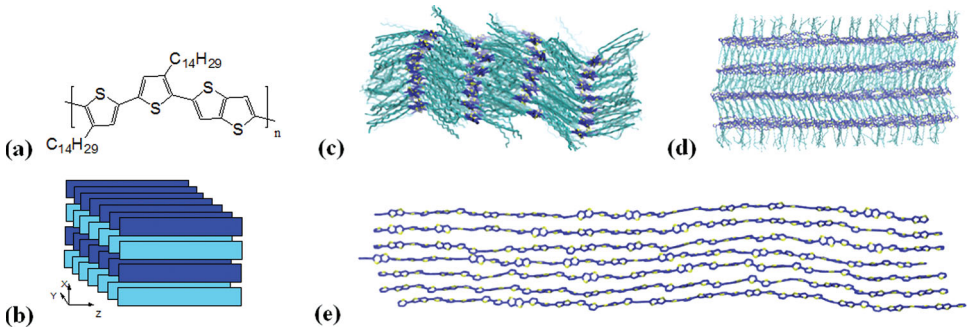


**Figure 1.** a) Chemical structure of PBTTT and b) schematic diagram of 7 × 4 arrangement PBTTT chains in the simulation box. c–e) Snapshots ($t$ = 90 ns) of the simulation in the $xy$, $xz$, and $yz$ planes. Hydrogen atoms are omitted, carbon/sulfur atoms on the backbone are in blue/yellow, and carbon atoms on the interdigitated alkyl chain are in cyan.

comparison to P3HT is a result of improved structural ordering rather than being an intrinsic property of crystalline regions of the polymer. Moreover, he found that the rotation of the conjugated planes around the polymer axis is energetically favorable, which reduces the electron and hole bandwidths and opens up the energy gap between occupied and empty states. From quantum mechanical calculations, Medina et al.[21] confirmed that the hole mobility of the polymer is prevalently determined by the actual packing of the polymer instead of the energetic parameters such as internal reorganization energy or the nature of the repeat unit. Poelking et al.[22] suggested that the efficient charge transport is related to high and fast dynamic electronic coupling and small energetic disorder by combining MD simulation (with the OPLS-AA force field) and quantum chemical calculations. Do et al.[23] used a similar force field to show that the structural properties of PBTTT facilitate both intra- and inter-chain charge transport due to a great degree of planarity, closer and more parallel stacking of the thiophene and thienothiophene rings, and interdigitation of the side chain. Cho et al.[12] also achieved the similar conclusion that the efficient intra- and inter-chain charge carrier transport is possible because of the high-structural ordering by MD simulations with the Universal Force Field. In relation to the existing works, the main difference introduced here is that we will not limit ourselves to the computation of the interaction between fragments of the system but we will compute the one-electron states for the full lamella, accessing for the first time the density of states and localization characteristics of the orbitals in the crystalline portions of PBTTT.

The study of the geometrical distortions of semicrystalline polymers with molecular dynamics is simplified by the knowledge of the unit cell of the system.[18,20,22] More importantly, Rivnay et al.[24] quantified the degree of paracrystalline disorder in the $\pi$ stacking direction with X-ray line-shape analysis, an information that can be of great importance to validate the structural model and that was already used to infer a relation between this type of disorder and a tail of trap (or defect) states with a breadth of 0.1 eV using density functional theory calculations.[24] Additional information concerning the trap states derives from the modeling of the transfer curves in thin film transistors.[2] The energy range of the trap states extracted from these models is directly related to the assumptions on the shape of the density of state and the mobility mechanism. The most common model used to characterize the defects in semicrystalline polymers assumes that the density of states decreases exponentially from the band edge of the ideal system and that the carriers are completely trapped in the band tail and moves with high mobility within the band.[6] According to this model, the thermal activation observed experimentally results from the transition from the defect states to energy below (for the hole) the mobility edge. The fitting of the experimental transfer curves is consistent with a density of states decreasing as $\approx\exp(-E/E_b)$ where $E_b$ is close to 30 meV for P3HT and PBTTT.[13] The typical energy difference between the Fermi level and the mobility edge in a working device is close to 0.1 eV.[6]

The main advantage of a microscopic modeling of the density of states is that the assumptions implicit in mobility edge models are automatically tested. Moreover, computing the dynamic density of states is that we can also access the lifetime of the trap states, that is, for how long a trap state, formed by a local deformation of the polymer structure, is located in the same position.

## 2. Methods

### 2.1. Computational Details

The simulated system contained 28 chains of PBTTT, each consisting of 12 PBTTT monomers, arranged into 4 lamellae, each containing 7 $\pi$–$\pi$ stacked chains (See Figure 1). The side chains were (initially) fully extended and interdigitated and periodic boundary conditions were used. The experimental triclinic crystal structure of PBTTT as reported in ref. [12] was used to define our initial structure. However we defined a super cell with unit vectors $c = 2c'$, $b = 2c' + 7b'$, $a = a'$ (where $a'$, $b'$, $c'$ are the original triclinic crystal unit cell parameters) to have a fully equivalent system with a quasi-orthorhombic unit cell, which allows better performances in large scale MD simulations. The separation between chains in the same layer was initially 3.68 Å ($\pi$–$\pi$ stacking distance), whereas the interlayer spacing (d-spacing) was 21.5 Å. The force field employed in this work is derived from the paper by Moreno et al.[25] on alkylthiophene-based oligomers and polymers, referred as FF3 in the original paper, complemented with an additional dihedral

angle parameters describing the torsion between thiophene and thienothiophene which was missing in the original reference. This parameter was obtained by using potential energy scans with quantum chemical calculations as described in the Supporting Information. The MD simulation was performed using constant NPT-MD simulations at 300 K and a pressure of 1 atm. (Temperature and pressure were controlled using a Nosé–Hoover thermostat and barostat (anisotropic), with relaxation times of 0.1 and 1 ps respectively). Simulation consisted of 50 ns of equilibration and 40 ns of data gathering (time step was 1 fs). All MD simulations were performed using the LAMMPS simulation package.[26]

The most computationally expensive step is the repeated calculation of the electronic structures of the individual lamella (each lamella contains 84 monomers) of PBTTT with periodic boundary condition, using structures extracted from the MD simulation at different times. A number of alternative methods have been proposed to deal with these large scale calculations including ad hoc charge patching methods[27] and fragment molecular orbital method.[28] Here, we consider the general SCC-DFTB (self-consistent charge density functional tight-binding) method based on a second-order Taylor expansion of the total DFT energy with respect to density fluctuations around a suitable reference density as implemented in the DFTB+ code.[29,30] The electronic coupling between lamellae has been neglected (it appears to be truly negligible from band structure calculations)[20] and the $C_{14}H_{29}$ alkyl chain was replaced with a $CH_3$ termination (an approximation tested in the literature).[19] In all of these calculations, SCC-DFTB convergence criteria of $10^{-5}$ atomic units is used. It has been confirmed that SCC-DFTB is about three orders of magnitude faster than full DFT method.[31] Some tests on the similarity of results between SCC-DFTB and more conventional B3LYP/6–31G* calculations are reported in the Supporting Information.

### 2.2. Analysis

The main results are presented in terms of the density of states (*DOS*) and three measures of the orbital localization: the localization length (*LL*), the inverse participation ratio per monomer ($IPR_M$) and inverse participation ratio per chain ($IPR_C$).

The *DOS* for one lamella can be defined as

$$\rho(E) = \sum_m \delta(E - E^{(m)}), \tag{1}$$

where $E^{(m)}$ is the energy of the molecular orbital $m$ for each lamella.

Indicating with $C_i^{(m)}$ the coefficient for atomic orbital $i$ for molecular orbital $m$, the normalization condition implies $\sum_{ij} C_i^{(m)} S_{ij} C_j^{(m)} = 1$ where $S_{ij}$ is the atomic orbital overlap matrix. If a lamella is partitioned into monomers, the weight of molecular orbital $m$ on a given monomer $k$ can be calculated by

$$P_k^{(m)} = \sum_{\substack{i \text{ on monomer } k \\ i \text{ on any monomer}}} C_i^{(m)} S_{ij} C_j^{(m)}, \tag{2}$$

$P_k^{(m)}$ represents the weight of molecular orbital $m$ on monomer $k$ ($\sum_k P_k^{(m)} = 1$) and can be used to quantify the molecular orbital position and its shape in a coarser way than $C_i^{(m)}$. Indicating with $r_k$ the centre of mass of monomer $k$, the centroid of the molecular orbital $m$ can be defined as $R^{(m)} = \sum_k r_k P_k^{(m)}$ and the localization length for molecular orbital $m$ can then be defined as

$$LL^{(m)} = 2\left(\sum_k |r_k - R^{(m)}|^2 P_k^{(m)}\right)^{1/2}. \tag{3}$$

The computations of $R^{(m)}$ and $LL^{(m)}$ were performed after the periodic system was redefined in such a way that $R^{(m)}$ was far from the boundary of the periodic box and the distance $|r_k - R^{(m)}|$ was measured with the minimum image convention. To better represent $LL^{(m)}$ at different orbital energies, an energy-dependent localization length is defined as

$$LL(E) = \sum_m LL^{(m)} \delta(E - E_m) / \sum_m \delta(E - E_m). \tag{4}$$

The inverse participation ratio per monomer, $IPR_M^{(m)}$, represents the number of monomers that shares a given orbital $m$ and it can range between 1 and the number of monomers of the system:

$$IPR_M^{(m)} = \left(\sum_k (P_k^{(m)})^2\right)^{-1}. \tag{5}$$

It is also of interest to consider a measure of how many chains in the same lamella share a given orbital $m$ defining the inverse participation ration per chain as

$$IPR_C^{(m)} = \left(\sum_l \left(\sum_{k on chain l} P_k^{(m)}\right)^2\right)^{-1}, \tag{6}$$

where $l$ is an index that runs on the chains and $IPR_C^{(m)}$ can take a value between 1 and the number of chains (7 in this case). As for the localization length, it is convenient for representation purposes to show the inverse participation ratios as a function of the orbital energy by defining the energy-dependent quantities

$$IPR_M(E) = \sum_m IPR_M^{(m)} \delta(E - E_m) / \sum_m \delta(E - E_m), \tag{7}$$

$$IPR_C(E) = \sum_m IPR_C^{(m)} \delta(E - E_m) / \sum_m \delta(E - E_m). \tag{8}$$

The results in the next section have been obtained with the Dirac delta function in Equations 1,4,7,8 approximated with a Gaussian with standard deviation 0.08 eV.

## 3. Results

### 3.1. Geometric Structure

Different views of the PBTTT structure after 90 ns MD simulation are shown in Figure 1. The average density is 1.06 g $cm^{-3}$, which agrees well with the experimental value 1.09 g $cm^{-3}$.[12] The intergiditated structure can be observed in Figure 1c,d for the entire simulation leading to a d-spacing (19.6 Å) between

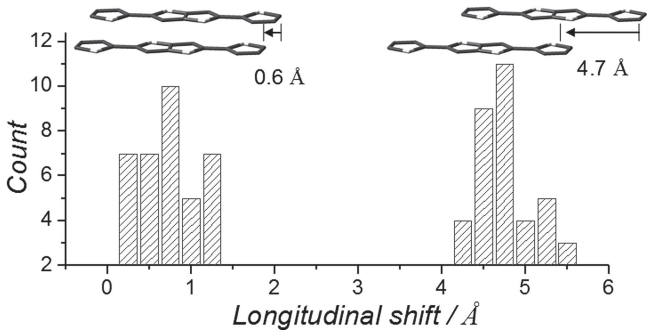


**Figure 2.** Distribution of the longitudinal shift, defined as the relative displacement of the thiophene centre along the direction of the PBTTT chain. Two distinct relative alignments are evident.

the lamellae which is narrowly distributed, consistent with experimental value (21.5 Å). The separation between chains along the $\pi$–$\pi$ stacking separation after 90 ns MD simulation is slightly larger (0.5 Å) than the experimental value. Figure 1e also shows that the thienothiophene rings are rotated out of the quasi-plane formed by bithiophene rings about ±45° (the actual dihedral distribution function is given in the Supporting Information).

PBTTT structure is often described in terms of lateral (along $x$ axis) and longitudinal (along $z$ axis) shifts of adjacent chains to show the disorder of the chains in different directions. In the absence of shift the chains would be perfectly paired with minimal distance between symmetry equivalent atoms. We observed lateral and longitudinal shifts of 1.7 ± 0.8 and 2.6 ± 2.1 Å respectively (shown as Figure 1d,e, calculated by MD snapshot at $t$ = 90 ns), which is consistent with the shifts (lateral and longitudinal shifts are 1.2 and 3.9 Å respectively) reported by Brocorens on the basis of molecular mechanics optimizations using UFF force field.[32] However, we have noted that the longitudinal shift is not normally distributed but there are two local minima in the system, as illustrated in **Figure 2**. The thienothiophene unit can either be adjacent to another thienothiophene unit in the closest chain or to a thiophene unit. The existence of these multiple energy minima is ultimately responsible for the disorder in the $\pi$–$\pi$ stacking direction.

In agreement with what reported by Salleo's group,[24] the high order of PBTTT is due to its interdigitation which locks the inter-lamellae spacing while the disorder along the $\pi$–$\pi$ stacking direction is considerable and comparable to what observed for example in P3HT. To verify that our structural model presents a level of disorder in the $\pi$–$\pi$ stacking direction comparable with what was inferred by the experiment we computed the paracrystallinity parameter $g$ by

$$g = \left( \frac{\langle d^2 \rangle}{\langle d \rangle^2} - 1 \right)^{1/2} \quad (9)$$

where $d$ indicates the distance between PBTTT chains in the same lamella measured in different positions. The method used to measure the distance $d$ from our coordinates is illustrated in **Figure 3**a. The polymer chains in a plane are approximated by a curve obtained by spline interpolation of the thienothiophene

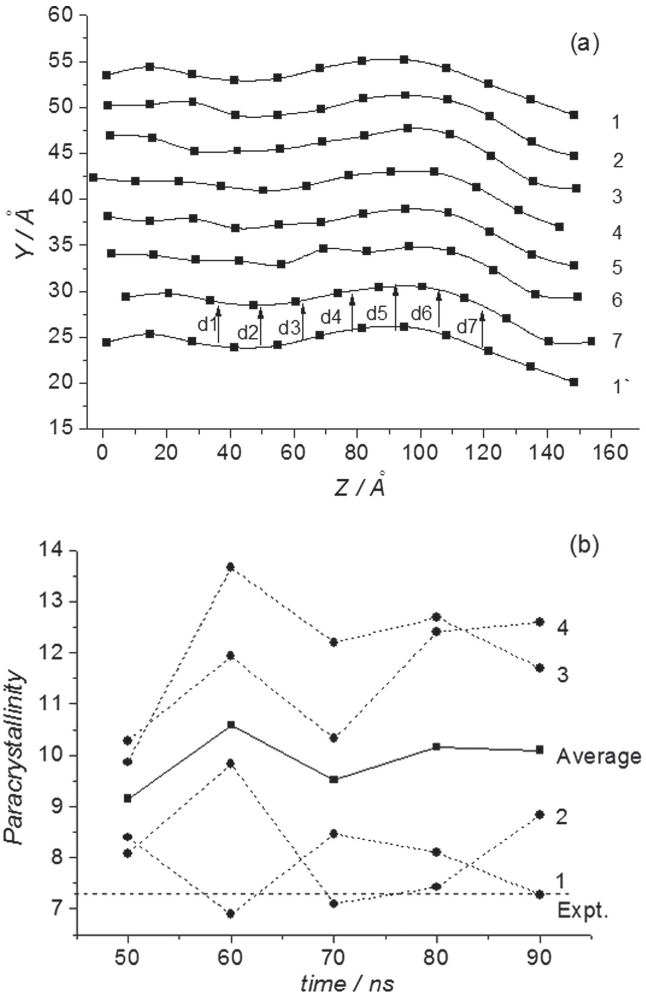


**Figure 3.** a) ■ represents the centroid coordinates of thienothiophene rings of the polymer chains including 8 $\pi$–$\pi$ stacking layers, chain 1` is chain 1 in the next unit cell. Black line is the spline fitting of the coordinates of polymer chain. b) Average (solid line) and separated (dashed line, 1, 2, 3, and 4) lamellae paracrystallinity parameter g for snapshots at t = 50, 60, 70, 80, 90 ns together with the experimental value.

centroids. Several distances have been measured for each pair of adjacent chains in the simulation as shown in Figure 3 and averaged according to Equation 9 to provide the paracrystallinity for each lamella at different simulation time. The results shown in Figure 3b indicate a large spread of paracrystallinity parameters among different lamellae. Our average paracrystallinity parameter is 9.9 ± 0.5 (0.5 is the standard deviation) which is not far from the experimentally reported value of 7.3 ± 0.7,[24] also considering the very different ways these parameters have been obtained. In fact, it should be noted that systematic errors are also possible in the experimental evaluation of the paracrystallininty from X-ray scattering profiles because the model used to derive $g$ makes the assumption of uncorrelated disorder between the distances, an assumption that may alter the results of the derived value for $g$. A better comparison could be based on the actual simulation of the X-ray scattering profile for the large model, which, however, would require a dedicated work.

In summary, the structural model of the semicrystalline polymer seems sufficiently accurate for the evaluation of the electronic structure, especially considering that it was obtained without any parameter adjusted to match the experimentally available structural data. This model seems to have slightly weaker $\pi$–$\pi$ interaction and a slightly higher disorder in the same direction than what can be argued from paracrystallinity measurements. Fortunately, as it will be clear in the next section, the main observations of this paper would be even strengthened if the actual structure of PBTTT were more ordered than what is predicted by the model.

For completeness, it is important to compare our results with the MD simulation of PBTTT presented in the literature.[22] The most relevant difference is that the simulation of this study[22] predicts a much ordered structure at room temperature with all side chain in trans configuration. A direct consequence of this effect is a much ordered structure in the lamellae with a computed paracristallinity that shows a systematic error in the opposite direction than ours (they computed it to be 3.7%). There are two possible sources of the discrepancy. It is possible that our simulation is representative of a "glassy" state that is not given the time to relax to its lowest free energy structure (which may or may not be achieved in the experimental timescale). So, one possibility is that the experimental paracristallinity is actually representative of a partially relaxed structure if the force field is sufficiently accurate and the "true" situation is intermediate between that proposed by the two models. Another possibility is that the difference between force fields is sufficient to allow in our case (but not in the case of the mentioned work)[22] the presence of two minima in the inter-chain interaction (as described in Figure 2) which promotes frustration in the structure and therefore a greater disorder. An experimental indication from infra-red spectroscopy that a small fraction of gauche defects are present also at room temperature in the most ordered phase is given elsewhere[33] but a quantitative analysis is difficult from the available experimental data. Such comparison highlights the difficulty of building structural models for polymers with this complicated chemical structure and the necessity of incorporating considerable experimental input in the computational models.

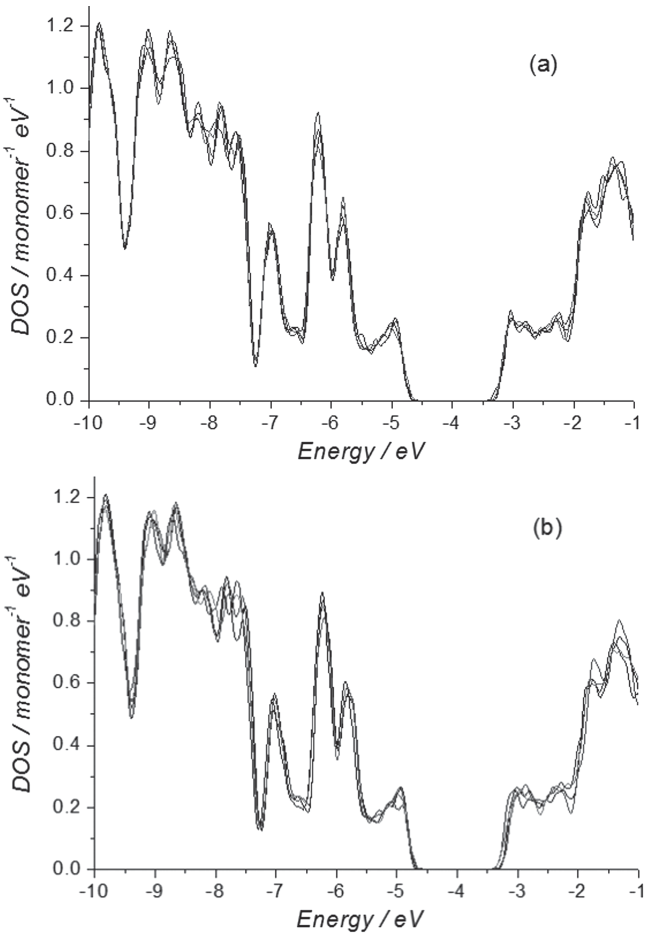


**Figure 4.** a) *DOS* of PBTTT for four different snapshots of the MD simulation for a certain lamella b) *DOS* of PBTTT for one snapshot of the MD simulation for four different lamellae separately. Broadening used to define *DOS* is 0.05 eV.

### 3.2. Electronic Structure

The DOS of four lamellae and the DOS of a specific lamella at different snapshots (60, 70, 80, 90 ns) are shown in **Figure 4**. The strong similarity between the curves is a reflection of the fact that the system is sufficiently large that the electronic structure of a single lamella at a given time is already representative of the DOS obtained averaging over many snapshots and lamellae (which is used in subsequent analysis). This seems to be true despite the fact that the lamellae display a rather independent dynamics and have different order parameters as highlighted in Figure 3b. The computed band gap of 1.6 eV is slightly underestimated with respect to the experimental value of about 2.1 eV,[11,34] a systematic error typical of most DFT methods that has little effect on our main analysis. In fact, we are going to focus in the remainder of this paper on the orbitals and their localization at the edge of the valence band (the results refer to averages over 4 lamellae and 4 snapshots).

**Figure 5** compares *DOS*, *LL(E)*, $IPR_M(E)$, $IPR_C(E)$ in a broad energy range and provide additional detail within the range of interest between –5.0 eV and –4.7 eV. Few orbitals are represented in **Figure 6** to exemplify the results of the statistical analysis. As shown in Figure 5 by both *LL(E)* and $IPR_M(E)$, the orbitals close to the valence band edge, at about –4.7 eV, are localized on a few (six-seven) monomers (see also Figure 6a). The localization length and the inverse participation increase rapidly to –5.0 eV where the first peak of the *DOS* is encountered. As one can see in Figure 6b, the orbitals at energy close to –5.0 eV are delocalized over a large fraction of the system. Under this condition the localization length does not have a physical meaning and it is actually determined by the size of the model used (see below for a discussion of possible polaronic effects).

The most striking element of the data in Figure 5 is that both $IPR_M$ and *LL* increase very rapidly within thermally accessible energies. On the contrary, a similar calculation on an amorphous polymer resulted in localization length only weakly

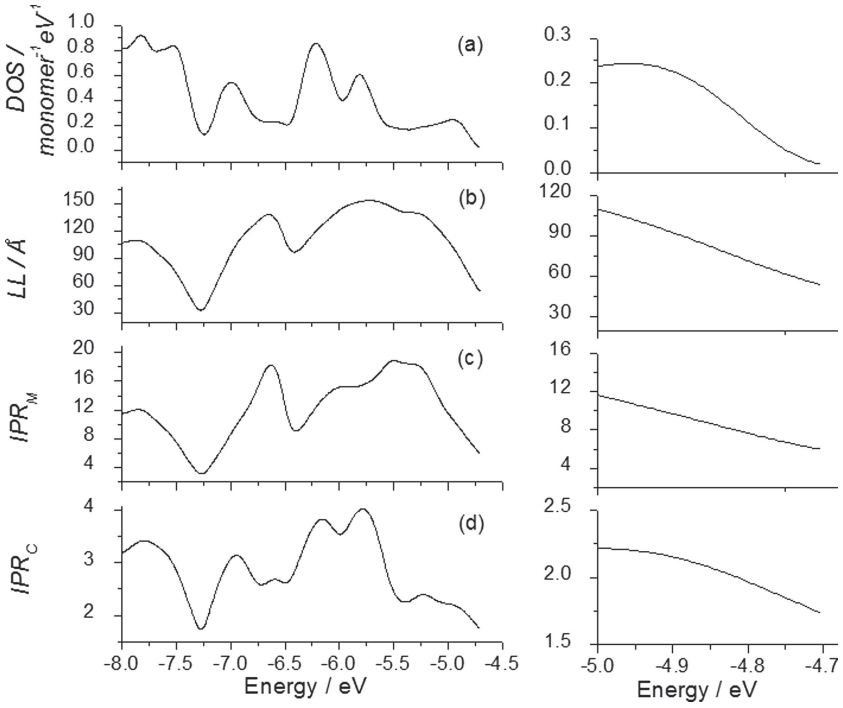


**Figure 5.** Comparison of the average a) *DOS*, b) *LL*, c) $IPR_M$, and d) $IPR_C$ of PBTTT as a function of orbital energy at the valence band (left) and zoom in the valence band edge region (right). The average include all eigenstates of different snapshots at $t$ = 60, 70, 80, and 90 ns for four lamellae.

dependent on the energy.[35] Clearly this means that localized traps states can access thermally much more delocalized states. These results obtained from atomistic calculations coincide in spirit with the phenomenological model of multiple trap and release transport, where it is assumed that a mobility edge exists such that for hole energies above a threshold the holes move in delocalized states and below that threshold the holes are stationary.[6] The comparison with the mobility edge model, however, cannot be pushed too far. In fact, while on one hand we agree with the mobility edge model in the sense that we see more localized states at the band edge, on the other hand we disagree for the fact that there is no sharp separation between localized and delocalized states. In the energy region of interest the states becomes gradually more delocalized as we move away from the band edge. The same qualitative features of mobility edge model (thermal activation and increased mobility with increased charge density) are expected for this energetic landscape where there is no actual "edge". Some arbitrary definition of this edge can be used to allow the comparison between materials and can be based either on a maximum localization length or minimum hole energy for a state to be defined as trap. For polymers we find useful to consider hole "traps" all states above the highest energy valence band DOS maximum (at –4.9 eV for PBTTT) as these are the states generated by the chain disorder and this is the (arbitrary) criterion used here. These states are delocalized over 10 monomers or less (according to $IPR_M$). The number of so-defined trap states is not high for a given lamella (on average 4 of such states are present per lamella) and so it is not possible to clarify whether the DOS tail is more exponential or Gaussian. Moreover, given the low density of "trap" states it is less likely that the carriers diffuse by hopping among quasi degenerate states (they are relatively far one from each other). The density of trap states computed by this model ($\approx 1 \times 10^{13}$ cm$^{-2}$) is of the same order of magnitude of the value inferred by electrical measurements fitted with multiple trap and release model ($\approx 5 \times 10^{13}$ cm$^{-2}$).[13]

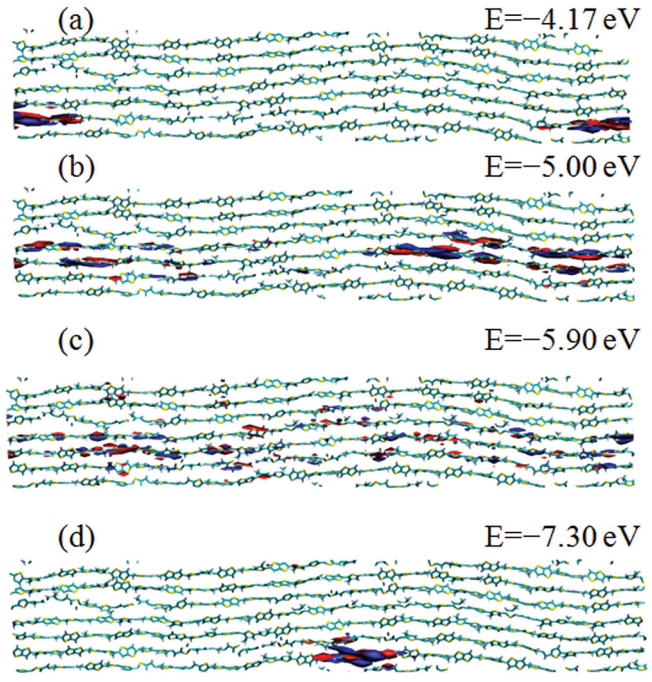


**Figure 6.** The orbital density positions, shapes, with energies of selected orbitals of PBTTT at t = 60 ns of the MD simulations.

One rather unexpected result of this calculation is that the orbitals show a rather large delocalization across the chains. This was not observed in P3HT and indicates that the structure of PBTTT favors cross-chain conjugation beyond what is normally expected in polymeric chains. $IPR_C$, a measure of how many chains share the orbital, is close to 2.0 at the band edge and can increase up to 4.0 far from the edge (an example of large cross-chain delocalization is given in the Figure 6c). An important consequence of this observation is that the inter-chain coupling in PBTTT is sufficiently strong that hopping models for inter-chain transport may fail.[36] Finally, an observation of no relevance for the transport mechanism but of potential theoretical interest is that, according to the data in Figure 5, the orbitals become localized again at around –7.3 eV, which also can be seen from Figure 6d. Simple one-dimensional models of a disordered chain can be built[37] to show that localized states are to be expected in the high energy and low energy

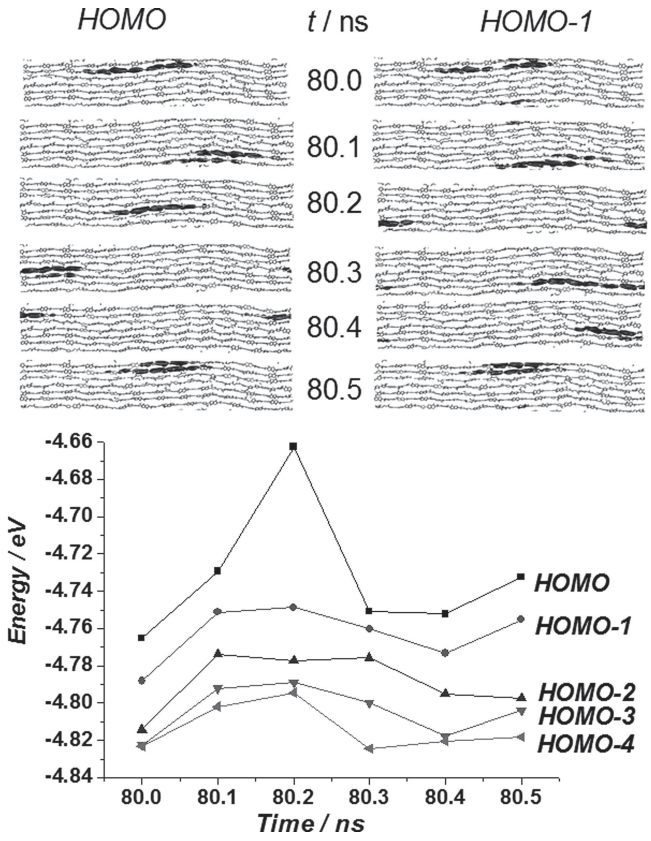


**Figure 7.** (Top) The orbital density positions and shapes of HOMO and HOMO–1 as a function of MD simulation time between 80.0 to 80.5 ns with a gap of 0.1 ns. (Bottom) The energy level of orbital HOMO–n (n = 0–4) as a function of MD simulation time in a lamella between 80.0 to 80.5 ns with a gap of 0.1 ns.

edges of the band (the region around –7.3 eV corresponds to the low energy edge of the band).

When we performed a similar study for P3HT we observed that the trap states are stationary in time,[18] that is, they are found in the same location for tens of nanoseconds and behave therefore as "static" traps from the point of view of the electron. The opposite conclusion was reached by monitoring the localization of the highest occupied orbitals in each lamella (the deepest trap) as a function of time. In **Figure 7** (top) we show the HOMO and HOMO–1 for 6 snapshots separated by 0.1 ns (an identical behavior was observed for other portions of the trajectory, reported in the supporting information). One can observe that these orbitals are localized in different regions of space that do not repeat over the course of the observation. The phenomenon is not too surprising as the band-width of PBTTT is narrower than P3HT (because of the co-polymer structure) and it is more likely that the relative energy of orbital localized in different regions of space changes over a short time. Figure 7 (bottom) shows that, indeed, the energy variation of the highest occupied orbitals in each lamella is comparable to the energy separation between these orbitals. The important point is, however, that the time scale for the orbital energy drift is comparable with the timescale for the charge diffusion and this may have a very large impact on the nature of charge transport. The traps, imposed by local deformations, are not static but "heal" with time and the trapped hole may be released as an effect of polymer dynamics without overcoming the energetic barrier. Finally, energy drift of the orbital is accompanied by some orbital change of shape that results for example in slightly higher or lower delocalization length as observable in snapshots at 80.0 and 80.5 ns in Figure 7.

The behavior described above was not found for other polymers but it is relatively common in many charge transfer donor–acceptor systems where it is referred to as conformationally gated electron transfer. In these systems it is the molecular conformation, controlled by the interaction of the system with the thermal bath, that determines the rate of electron transfer and not the intrinsic electron transfer rate at fixed configuration.[38–40]

The self-healing properties of PBTTT and the rapid delocalization of the wavefunction with increasing energy are probably both effects of the property of PBTTT of avoiding the formation of deep traps. The chemical origin of this property is not completely clear but it may be due to the electronic structure of the valence band of the polymer, which is largely determined by the orbital localized on the thienothiophene units weakly coupled by the mediation of the bithiophene units. In P3HT,[18] we observed that trap states were formed in regions where the polymer was more planar than the average while we did not observe any correlation between the local planarity of the chains and the localization of the highest occupied orbital. It can be speculated that there are no accessible distortions of the PBTTT chain that support localized states and this may be the key for its very high mobility.

It may be interesting to compare the approach proposed here with Poelking et al. work[22] focused on the same material. There, a set of assumptions have been made to make a connection between an atomistic picture and the observed charge mobility. Some of the assumptions (partitioning of the system into tetramers, partitioning in tetramer, validity of Marcus theory) may not be fully valid but they allow the computation of an important experimental observable. In our paper by computing the system eigenstates, we instead clarify what are the best orbitals that can be used as a basis to describe transport and what is their energetic distribution. On the other hand it is not possible within this scheme to go as far as computing the mobility because it is not trivial to derive hopping rates from eigenstates of the total system (being eigenstates they are adiabatic, i.e., non-interacting). Similarly, it is not easy to expand Marcus theory to the situation of strongly interacting inter-chain (and sometime cross-chain) fragments. The two approaches as they stand are incomplete but it is conceivable that a synthesis of the two (e.g., a hopping model based on the system eigenstates) can be achieved in the future. The results of this paper suggest that a useful quantitative transport model for this class of materials would involve a series of incoherent hops but with the characteristic that higher energy states are more delocalized and that the carriers can travel longer distances by hopping into these partially delocalized states.

One important aspect that goes beyond the scope of this work but that we would like to discuss briefly is the effect of the electron–phonon coupling on the nature of the electronic states discussed in this paper. In systems with weak electronic coupling

small polarons localized on individual molecules or monomers could be formed.[41] Much more frequently, especially in polymers, the polarons extend over many tens of monomers and their size is difficult to evaluate because it may extend beyond the size achievable for electronic structure optimizations of charged systems.[17] The electron–phonon coupling for PBTTT has been evaluated in ref.[22] which reported the reorganization energy for the charge hopping in oligomers containing from 1 to 6 oligomers. The data suggests that the polaron size for these systems in the absence of disorder is well above 6 monomers. This means that the more localized trap states determined in this paper are unlikely to be changed in size or localization by the electron-phonon coupling. This is very much in agreement with the conclusion that the room temperature mobility in semicrystalline pBTTT is not limited by polaron localization based on charge modulated spectroscopy measurements.[42] On the other hand the localization of more delocalized states will be likely corrected (and reduced) by the effect of the electron-phonon coupling term. To the best of our knowledge computation of electron-phonon coupling on atomistic model of this size has never been attempted because the presence of many quasi-degenerate polaronic states lead to an extremely complicated potential energy surface.

## 4. Conclusions

In this paper, we have used a combination of large scale electronic structure calculations and molecular dynamics simulations to investigate the nature of the one-electron states responsible for hole transport in the high mobility semiconducting polymer PBTTT. The validity of the structural model was established by comparison with the available data from crystallography and from the inferred paracrystallinity parameters. The electronic structure of the entire lamella was achievable by adopting the approximate DFTB methodology. While several technical difficulties make this study rather challenging from the computational point of view the analysis of the results is extremely straightforward and the results are very revealing. We have looked at the localization characteristics of the states at the edge of the valence band, at their local geometry and their time evolution. The results, especially when compared with the behavior of other polymers like P3HT, clearly point to some of the characteristics of PBTTT that are at the origin of its improved mobility: i) The one-electron states become very rapidly delocalized within few $k_BT$ from the valence band edge, that is, there is a very low density of states that can be considered as trap states. Using the language of multiple trap and release model the mobility edge is very close to the valence band edge. ii) A very large delocalization of states across chain is observed, which also increases as states deeper in the valence band are considered. It seems that also the transport across chains may be described by mechanisms that invoke partial delocalization while it was generally assumed that cross-chain transport occurs via incoherent hopping. iii) The traps, determined by local distortions of the chain, have a typical lifetime of less than 0.1 ns, that is, the conformational changes of the polymer due to its thermal fluctuations can be sufficient to induce a detrapping of the charge carrier.

In agreement with what has been observed by Salleo's group,[24] we do not see that the individual lamella is more ordered than P3HT (the interdigitation stabilizes the interlamellae distance but does not create more ordered chains). The improved properties of PBTTT are therefore due to its electronic structure that prevents the chain distortions from forming long lived trap states.

Interestingly, on one hand the static description of the density of states and localization length supports the phenomenological transport model of multiple trapping and release.[43] On the other hand, the existence of a short lifetime for the geometric traps suggests that the activation energy for detrapping the carrier can be smaller than expected or that what appears to be an activation energy for detrapping is instead an activation energy for conformational changes.[44] The results discussed in this work are all determined by the initial decision to compute the electronic structure of the full lamella without imposing a partitioning of the system into its monomers. We are inclined to think that this approach may be beneficial, when extended to a broader range of polymers, to understand the relation between their atomistic structure and their electronic properties. Alternatively, it is always possible to adopt a partitioning method[45–47] but it is advisable to include the coupling between fragments variationally as all the intra-chains coupling and some of the inter-chain couplings are too large for a perturbative treatment.

## Supporting Information

Supporting Information is available from the Wiley Online Library or from the author.

## Acknowledgments

This work was supported by ERC (MiMESIs). The authors are grateful to David Cheung, Migen Halo, Ting Qin, Rocco Fornari, and Alberto Salleo for useful comments and discussions. The authors are also grateful to Denis Andrienko for his insight on the comparison between this and one other work.[22]

Received: June 17, 2013
Revised: July 29, 2013
Published online: September 24, 2013

[1] A. Salleo, R. J. Kline, D. M. DeLongchamp, M. L. Chabinyc, *Adv. Mater.* **2010**, *22*, 3812.
[2] H. Sirringhaus, *Adv. Mater.* **2005**, *17*, 2411.
[3] M. Geoghegan, G. Hadziioannou, *Polymer Electronics*, Oxford University Press, Oxford, **2013**.
[4] N. Tessler, Y. Preezant, N. Noam Rappaport, Y. Roichman, *Adv. Mater.* **2009**, *21*, 2741.
[5] S. E. Baranovski, *Charge Transport in Disordered Solids with Applications in Electronics*, Wiley, West Sussex, **2006**.
[6] A. Salleo, T. W. Chen, A. R. Volkel, Y. Wu, P. Liu, B. S. Ong, R. A. Street, *Phys. Rev. B* **2004**, *70*, 115311.
[7] M. Caironi, M. Bird, D. Fazzi, Z. H. Chen, R. Di Pietro, C. Newman, A. Facchetti, H. Sirringhaus, *Adv. Funct. Mater.* **2011**, *21*, 3371.
[8] H. Sirringhaus, P. J. Brown, R. H. Friend, M. M. Nielsen, K. Bechgaard, B. M. W. Langeveld-Voss, A. J. H. Spiering, R. A. J. Janssen, E. W. Meijer, P. Herwig, D. M. de Leeuw, *Nature* **1999**, *401*, 685.

[9] I. McCulloch, M. Heeney, C. Bailey, K. Genevicius, I. MacDonald, M. Shkunov, D. Sparrowe, S. Tierney, R. Wagner, W. Zhang, M. L. Chabinyc, R. J. Kline, M. D. McGehee, M. F. Toney, *Nat. Mater.* **2006**, *5*, 328.
[10] B. H. Hamadani, D. J. Gundlach, I. McCulloch, M. Heeney, *Appl. Phys. Lett.* **2007**, *91*, 243512.
[11] D. M. DeLongchamp, R. J. Kline, E. K. Lin, D. A. Fischer, L. J. Richter, L. A. Lucas, M. Heeney, I. McCulloch, J. E. Northrup, *Adv. Mater.* **2007**, *19*, 833.
[12] E. Cho, C. Risko, D. Kim, R. Gysel, N. C. Miller, D. W. Breiby, M. D. McGehee, M. F. Toney, R. J. Kline, J.-L. Bredas, *J. Am. Chem. Soc.* **2012**, *134*, 6177.
[13] C. Wang, L. H. Jimison, L. Goris, I. McCulloch, M. Heeney, A. Ziegler, A. Salleo, *Adv. Mater.* **2010**, *22*, 697.
[14] T. Lei, J.-H. Dou, X.-Y. Cao, J.-Y. Wang, J. Pei, *J. Am. Chem. Soc.* **2013**, *135*, 12168.
[15] C. B. Nielsen, M. Turbiez, I. McCulloch, *Adv. Mater.* **2013**, *25*, 1859.
[16] I. McCulloch, R. S. Ashraf, L. Biniek, H. Bronstein, C. Combe, J. E. Donaghey, D. I. James, C. B. Nielsen, B. C. Schroeder, W. Zhang, *Acc. Chem. Res.* **2012**, *45*, 714.
[17] S. S. Zade, M. Bendikov, *Chem. Eur. J.* **2008**, *14*, 6734.
[18] D. P. McMahon, D. L. Cheung, L. Goris, J. Dacuna, A. Salleo, A. Troisi, *J. Phys. Chem. C* **2011**, *115*, 19386.
[19] D. L. Cheung, D. P. McMahon, A. Troisi, *J. Am. Chem. Soc.* **2009**, *131*, 11179.
[20] J. E. Northrup, *Phys. Rev. B* **2007**, *76*, 245202.
[21] B. M. Medina, A. Van Vooren, P. Brocorens, J. Gierschner, M. Shkunov, M. Heeney, I. McCulloch, R. Lazzaroni, J. Cornil, *Chem. Mater.* **2007**, *19*, 4949.
[22] C. Poelking, E. Cho, A. Malafeev, V. Ivanov, K. Kremer, C. Risko, J.-L. Bredas, D. Andrienko, *J. Phys. Chem. C* **2013**, *117*, 1633.
[23] K. Do, D. M. Huang, R. Faller, A. J. Moulé, *Phys. Chem. Chem. Phys.* **2010**, *12*, 14735.
[24] J. Rivnay, R. Noriega, J. E. Northrup, R. J. Kline, M. F. Toney, A. Salleo, *Phys. Rev. B* **2011**, *83*, 121306.
[25] M. Moreno, M. Casalegno, G. Raos, S. V. Meille, R. Po, *J. Phys. Chem. B* **2010**, *114*, 1591.
[26] S. Plimpton, *J. Comput. Phys.* **1995**, *117*, 1.
[27] N. Vukmirovic, L.-W. Wang, *J. Chem. Phys.* **2008**, *128*, 121102.
[28] D. P. McMahon, A. Troisi, *Chem. Phys. Lett.* **2009**, *480*, 210.
[29] B. Aradi, B. Hourahine, T. Frauenheim, *J. Phys. Chem. A* **2007**, *111*, 5678.
[30] M. Elstner, D. Porezag, G. Jungnickel, J. Elsner, M. Haugk, T. Frauenheim, S. Suhai, G. Seifert, *Phys. Rev. B* **1998**, *58*, 7260.
[31] M. Elstner, *Theor. Chem. Acc.* **2006**, *116*, 316.
[32] P. Brocorens, A. Van Vooren, M. L. Chabinyc, M. F. Toney, M. Shkunov, M. Heeney, I. McCulloch, J. Cornil, R. Lazzaroni, *Adv. Mater.* **2009**, *21*, 1193.
[33] D. M. DeLongchamp, R. J. Kline, Y. Jung, E. K. Lin, D. A. Fischer, D. J. Gundlach, S. K. Cotts, A. J. Moad, L. J. Richter, M. F. Toney, M. Heeney, I. McCulloch, *Macromolecules* **2008**, *41*, 5709.
[34] Q. Sun, K. Park, L. Dai, *J. Phys. Chem. C* **2009**, *113*, 7892.
[35] T. Qin, A. Troisi, *J. Am. Chem. Soc.* **2013**, *135*, 11247.
[36] A. Troisi, *Organ. Electr.* **2011**, *12*, 1988.
[37] S. N. Evangelou, *J. Phys. C* **1986**, *19*, 4291.
[38] M. L. Paddock, M. Flores, R. Isaacson, C. Chang, E. C. Abresch, P. Selvaduray, M. Y. Okamura, *Biochem.* **2006**, *45*, 14032.
[39] V. L. Davidson, *Acc. Chem. Res.* **2008**, *41*, 730.
[40] B. Rabenstein, G. M. Ullmann, E.-W. Knapp, *Biochem.* **2000**, *39*, 10487.
[41] A. Troisi, *Chem. Soc. Rev.* **2011**, *40*, 2347.
[42] N. Zhao, Y. Y. Noh, J. F. Chang, M. Heeney, I. McCulloch, H. Sirringhaus, *Adv. Mater.* **2009**, *21*, 3759.
[43] A. Salleo, *Mater. Today* **2007**, *10*, 38.
[44] R. Zwanzig, *Acc. Chem. Res.* **1990**, *23*, 148.
[45] D. P. McMahon, A. Troisi, *Chem. Phys. Lett.* **2009**, *480*, 210.
[46] N. Vukmirovic, L. W. Wang, *J. Phys. Chem. B* **2009**, *113*, 409.
[47] T. Kubar, M. Elstner, *J. R. Soc. Interface* **2013**, *10*, 20130415.